INFECTIOUS DISEASE

Architectural immunity: Ants alter their nest networks to prevent epidemics

Luke Leckie[1,2,3]*, Mischa Sinha Andon[1], Katherine Bruce[1], Nathalie Stroeymeyt[1]*

In animal groups, spatial structure shapes social interaction patterns, thereby influencing the transmission of infectious diseases. Active modifications to the spatial environment could therefore be a potent tool to mitigate epidemic risk. We tested whether *Lasius niger* ants modify their nest architecture in response to pathogens by introducing control- or pathogen-treated individuals into nest-digging groups and monitoring three-dimensional nest morphogenesis. Pathogen exposure led to architectural changes, including faster nest growth, increased interentrance distance, transmission-inhibitory changes in nest network topology, and reduced chamber centrality. Simulations confirmed that these changes reduced transmission and highlighted a synergy between architectural and behavioral responses to disease. These results provide evidence for architectural immunity in a social animal and offer insights into how spatial organization can be leveraged to decrease epidemic susceptibility.

Animal and human networks influence the spread of disease from local to global scales. For instance, the properties of contact and social networks determine the risk and severity of epidemics within social groups (*1*–*3*); urban and metapopulation networks shaped by the layout of buildings, cities, and natural habitats influence social interaction and dispersal patterns and thus affect disease transmission dynamics (*4*–*7*); and global transportation networks facilitate the long-range transmission of disease by connecting distant populations (*8*).

There is increasing evidence that modifying social contact networks is an effective intervention strategy against epidemics that is used in a broad range of animal and human societies. Several species, including ants, humans, guppies, mice, and mandrills, are known to avoid infected conspecifics, thereby reducing disease transmission rates (*9*–*11*). Furthermore, ants and humans respond to pathogens by increasing the compartmentalization of their social networks to limit pathogen spread across the group (*2*, *12*). In addition to modifying their social networks, human societies have also used modifications to their spatial networks as an active means to reduce disease transmission (*13*). Historical examples include the expansion of urban spaces and the separation of cities into functional zones as preventative measures against outbreaks of the bubonic plague in the 1300s and cholera in the 1800s, respectively (*14*, *15*). More recently, active network–based interventions have been proposed that target the spatial properties of transport networks, city layouts, and building architecture to control modern human pandemics, such as COVID-19 (*6*, *14*, *16*, *17*). Yet, because of the lack of empirical data, it is still unclear which spatial interventions may be most effective at limiting pathogen spread while preserving the functioning of society. Animal societies that inhabit complex built structures could provide an opportunity to study evolved solutions to this challenge. However, there is, as yet, no evidence that nonhuman animals actively modify their spatial surroundings to mitigate epidemic risk, even though such interventions could be highly effective.

In this work, we investigate the possible role of architectural changes in nest layout as a disease defense strategy in the black garden ant *Lasius niger*. Nest-building social insects are an ideal system to explore for evolved architectural, disease-targeting interventions in animal societies. Because high interaction rates between related colony members favor the transmission of infectious pathogens, social insects have evolved a large suite of collective mechanisms for disease defense that confer "social immunity," including active modifications to colony social interaction networks (*2*, *18*). Furthermore, excavated ant nests can demonstrate a high degree of complexity, with specialized chambers housing food, brood, reproductive individuals, or waste connected by tunnels into underground networks that successfully isolate potential infectious sources (*19*, *20*). However, although previous work has indicated that excavation dynamics are influenced by abiotic stressors, such as temperature and soil composition (*21*–*25*), and by the presence of fungal spores in the soil (*26*), it is currently unknown whether ants respond to infectious threats by actively modifying their whole-nest architecture to reduce disease transmission. In this work, we test this hypothesis using a combination of pathogen exposure, video recording, x-ray micro–computed tomography (micro-CT), spatial network analysis, and agent-based simulations of disease transmission within nests.

Results

To investigate how pathogen exposure influences nest digging by *L. niger* ants, we allowed groups of 180 workers to excavate a new nest in a digging arena. One day after the onset of excavation, we introduced 20 additional workers, either exposed to the generalist entomopathogenic fungus *Metarhizium brunneum* (pathogen-exposed nests, $n = 10$) or treated with a sham solution (control nests, $n = 10$), into the digging arena. *M. brunneum* is a natural ant pathogen (*27*, *28*) that is picked up from the environment by contact with sporulating cadavers. Contaminated workers can transmit infectious spores to nestmates through physical contact for up to 1 day after exposure, ~90% of directly exposed workers die from infection within 10 days, and the mortality of nestmates increases by a factor of ~3 (*2*). After the introduction of the treated ants, we monitored nest excavation for 6 days using video recording of surface activity and nondestructive micro-CT scans of the internal nest structure (Fig. 1, A and B; movie S1; and materials and methods).

Pathogen exposure influences surface activity and surface properties of the nest

To investigate the influence of treatment on individual-level activity at the surface, we recorded the number of treated and untreated workers leaving the nest via the main (central) entrance (materials and methods). The exit rate of both untreated and treated workers decreased significantly over time in both treatments. However, whereas the exit rate of untreated workers was unaffected by treatment, treated workers exited the main nest entrance at a significantly higher rate in pathogen-exposed compared with control nests [fig. S1 and table S1; linear mixed-effects model (LMM), effect of time: untreated workers, $\chi^2 = 208.74$, df = 1, $P < 0.0001$; treated workers, $\chi^2 = 6.30$, df = 1, $P = 0.012$; effect of treatment: untreated workers, $\chi^2 = 0.021$, df = 1, $P = 0.89$; treated workers, $\chi^2 = 6.53$, df = 1, $P = 0.011$; interaction treatment × time: both untreated and treated workers, $\chi^2 \leq 2.11$, $P \geq 0.14$]. This indicates that pathogen exposure increases the surface activity of directly treated workers but not their nestmates. Because pathogen exposure does not lead to increased activity in this host-pathogen system (fig. S2), this likely reflects self-isolation by exposed workers outside the nest, as has already been reported in several species of ant, including *L. niger* (*2*, *11*, *29*). Furthermore, we found that entrances were spaced further apart from one another in pathogen-treated versus control nests (Fig. 2; LMM, effect of treatment throughout

[1]School of Biological Sciences, University of Bristol, Bristol, UK. [2]Department of Informatics, Luddy School of Informatics, Computing, and Engineering, Indiana University Bloomington, Bloomington, IN, USA. [3]Cognitive Science Program, Indiana University Bloomington, Bloomington, IN, USA. *Corresponding author. Email: lleckie@iu.edu (L.L.); nathalie.stroeymeyt@bristol.ac.uk (N.S.)

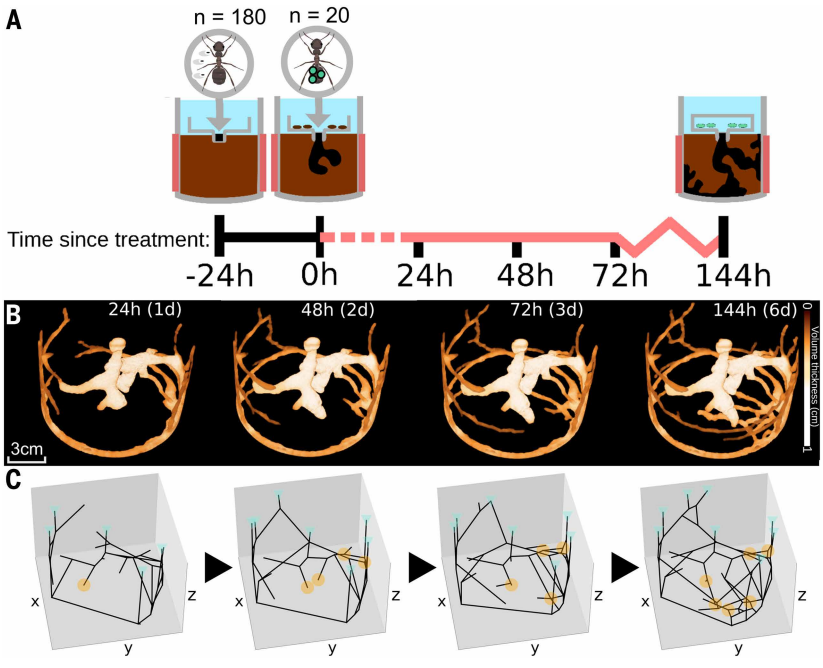

Fig. 1. Experimental protocol and nest network extraction. (**A**) One hundred and eighty ants with 25 mg of early-instar brood and 15 pupae were introduced into a soil-filled container (digging arena) and allowed to excavate a nest freely (−24 hours). After 24 hours, a CT scan of the nest was taken (baseline scan), and then 20 sham- or 20 pathogen-treated ants were introduced near the nest entrance (0 hour). Colonies were allowed to excavate the nest for 6 additional days, and CT scans were taken 24, 48, 72, and 144 hours (1, 2, 3, and 6 days) after treatment. Previous research has revealed no effects of repeated CT scanning on the excavation behavior of *Lasius* ants in a similar experimental setup (*22*). (**B**) CT scan reconstructions of nest volumes 1 day (24 hours), 2 days (48 hours), 3 days (72 hours), and 6 days (144 hours) after treatment. Volume thickness is encoded by increasing color brightness. (**C**) Three-dimensional (3D) spatial networks automatically extracted from the nest CT scans. Cyan triangles indicate nest entrances, orange circles indicate nest chambers, and black lines indicate tunnels (network edges).

experiment, $\chi^2 = 4.50$, df = 1, $P = 0.034$; Fig. 3A; LMM, effect at 6 days: entrances 0.62 ± 0.30 cm further apart in pathogen-treated nests, $\chi^2 = 5.93$, df = 1, $P = 0.015$). Increased spacing between entrances could lead to decreased contact rates between individuals at the surface and has been used as a strategy to mitigate disease transmission in human buildings (*30*).

Pathogen exposure influences overall nest growth

To study the influence of pathogen exposure on nest growth, we automatically identified nest chambers, entrances, tunnels, junctions, and dead ends from the micro-CT scans and measured their volumes (Fig. 1 and materials and methods). Analyses of nest properties in pre-exposure scans (0 hour) (i.e., before the introduction of treated ants) revealed no significant between-treatment differences, which indicates that any differences in post-exposure nests should be a result of pathogen exposure rather than random initial fluctuations between treatment groups (table S2).

Pathogen-exposed *L. niger* workers typically sharply decrease the amount of time that they spend inside the nest after exposure and slightly reduce their activity levels (fig. S2). Hence, if nest architecture changes as a passive consequence of infection, we would expect pathogen-exposed nests to grow more slowly than control nests (*31*). Conversely, because higher nest volumes should lead to lower ant density and thus fewer physical contacts, if the ants actively adjust their nest architecture to decrease transmission risk, we would expect pathogen-exposed groups to excavate nests at a faster rate. In agreement with the latter prediction, we found that the overall nest volume increased significantly faster in pathogen-exposed versus control nests (fig. S3; LMM, interaction treatment × time, $\chi^2 = 5.78$, df = 1,

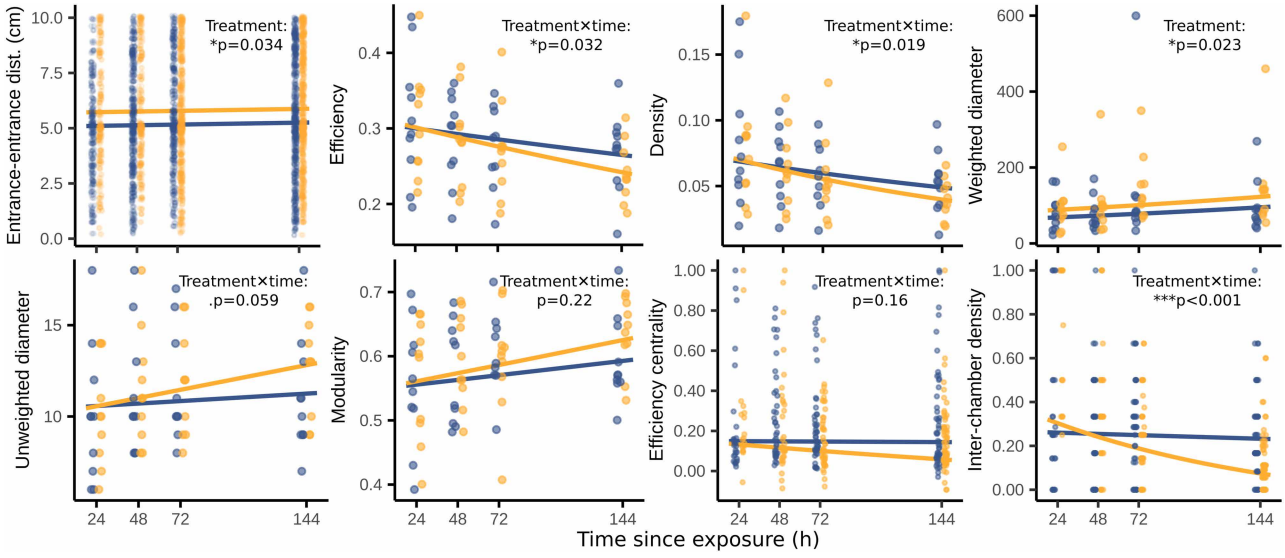

Fig. 2. Nest and chamber architectural properties as a function of time. Lines represent LMM fits for control (blue) and pathogen-treated colonies (orange), back-transformed where appropriate. Significance of the main treatment effect or the interaction between treatment and time (treatment × time) on a nest property are indicated on each graph. Original *P* values are provided, with an estimated study-wide false discovery rate (expected proportion of false positive results across all separate analyses) of 0.072 (~1 out of 14). For entrance-entrance distance, each point represents a pairwise measure of Euclidean distance between a new entrance and any other entrance ($n = 2529$ pairs). For efficiency, density, weighted diameter, unweighted diameter, and modularity, each point represents one nest ($n = 79$). For efficiency centrality and interchamber density, each point represents one chamber ($n = 336$). Efficiency, density, weighted diameter, efficiency centrality, and interchamber density were log-transformed for statistical analyses. Definitions of all properties are provided in Table 1, and model coefficients and exact *P* values are provided in table S1.

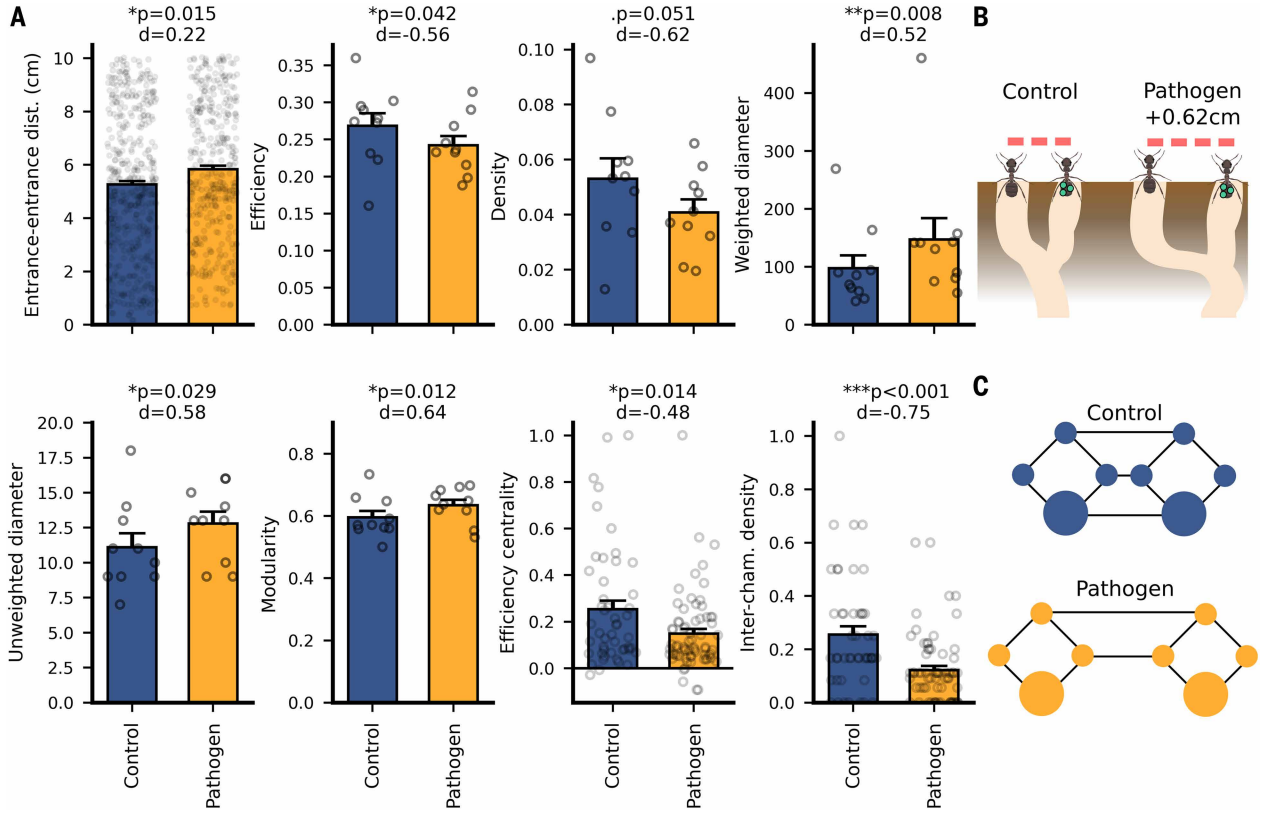

Fig. 3. Pathogen-induced architectural modifications 6 days after treatment. (**A**) Bars and whiskers show the means and standard errors for each property. Points represent individual data points [entrance-entrance distance (dist.): $n = 2529$ pairs of entrances; efficiency, density, weighted diameter, unweighted diameter, and modularity: $n = 20$ nests; efficiency centrality, interchamber density: $n = 336$ chambers]. Significance of the main effect of treatment at day 6 (LMM) and Cohen's d effect size (|d| ~ 0.2: weak effect; |d| ~ 0.5: medium effect; |d| ~ 0.8: strong effect) are indicated above each plot. Model coefficients and exact *P* values are provided in table S1. Original *P* values are provided, with an estimated study-wide false discovery rate (expected proportion of false positive results across all separate analyses) of 0.072 (~1 out of 14). (**B**) Illustration of entrance spacing mediating reduced interaction rate (not to scale). Entrances in pathogen-exposed nests (right) were spaced on average 0.62 cm (~1 to 1.5 *L. niger* worker body lengths) further apart compared with control nests (left), which could reduce the rate of interactions at the surface. (**C**) Simplified illustration of between-treatment differences in control (blue) and pathogen-exposed (orange) architectures after 6 days. Small circles represent junctions, large circles represent chambers, and black lines represent tunnels. Pathogen-exposed nests had higher (weighted and unweighted) diameter and modularity but lower density and network efficiency, and chambers had lower efficiency centrality and interchamber density.

$P = 0.016$), although this effect was too small to translate into significant between-treatment differences in nest volume by the end of the experiment (effect of treatment at 6 days, $\chi^2 = 0.23$, df = 1, $P = 0.63$). The faster growth of pathogen-exposed nests was not a result of a faster increase in the number and/or volume of nest chambers or in the number of nest entrances (fig. S3; LMM, interaction treatment × time, $\chi^2 \leq 1.80$, df = 1, $P \geq 0.18$, for all variables). Instead, pathogen exposure led to a significant increase in the rate of tunnel formation (fig. S3; LMM, interaction treatment × time, $\chi^2 = 5.49$, df = 1, $P = 0.019$), which suggests that it may affect the connectivity of the nest network.

Pathogen exposure influences the overall nest network topology

To test whether pathogen-exposed groups of *L. niger* workers alter the topology of their nest network to decrease epidemic risk, we identified properties known to influence disease transmission in social networks (*1*, *2*, *32*) (Table 1) and measured them in the spatial nest networks consisting of chambers, junctions, dead ends, and entrances (nodes) connected by tunnels (edges; Fig. 1C). We predicted that pathogen-exposed nest networks would display increased transmission-inhibitory properties and decreased transmission-enhancing properties compared with control nests.

In agreement with this prediction, we found that nest network efficiency and density (transmission-enhancing properties) decreased at a significantly higher rate in pathogen-exposed compared with control nests (Fig. 2; LMM, effect of treatment × time: efficiency, $\chi^2 = 4.58$, df = 1, $P = 0.032$; density, $\chi^2 = 5.52$, df = 1, $P = 0.019$). Both properties were reduced in pathogen-exposed nests by 6 days after treatment (Fig. 3A; LMM, effect of treatment at 6 days: efficiency, $\chi^2 = 4.125$, df = 1, $P = 0.042$; density, $\chi^2 = 3.82$, df = 1, $P = 0.051$). In addition, we found that the weighted diameter of the nest network (transmission-inhibitory property) was significantly higher in pathogen-exposed compared with control nests throughout the experiment (Fig. 2; LMM, effect of treatment throughout experiment, $\chi^2 = 5.17$, df = 1, $P = 0.023$; Fig. 3A; LMM, effect at 6 days, $\chi^2 = 6.97$, df = 1, $P = 0.008$). Furthermore, there were nonsignificant trends for the unweighted diameter and modularity of nest networks (transmission-inhibitory properties) to increase faster in pathogen-exposed versus control nests (Fig. 2; LMM, effect of treatment × time: unweighted diameter, $\chi^2 = 3.57$, df = 1, $P = 0.059$; modularity, $\chi^2 = 1.48$, df = 1, $P = 0.22$), and both properties were significantly higher in pathogen-exposed nests by the end of the experiment (Fig. 3A; LMM, effect of treatment at 6 days: unweighted diameter, $\chi^2 = 4.79$, df = 1, $P = 0.029$; modularity, $\chi^2 = 6.34$, df = 1, $P = 0.012$). No other transmission-relevant properties of the

Table 1. Summary of network properties measured from nest networks and their predicted effects on disease transmission. A plus sign (+) indicates enhancement, and a minus sign (−) indicates inhibition.

Global property	Definition—global network	Effect on transmission
Efficiency	Ability of the network to convey information quickly across all nodes	+ (*45*)
Density	Proportion of existing connections among all possible connections	+ (*46*)
Weighted diameter	Shortest weighted path length (i.e., sum of edge weights) between the two most distant nodes in the network	− (*47*)
Unweighted diameter	Shortest unweighted path length (i.e., number of steps) between the two most distant nodes in the network	− (*47*)
Modularity	Extent to which a network is divided into separate communities with many within-community and few intercommunity connections	− (*48*)
Clustering	Tendency of neighboring nodes to form fully connected sets	Context-dependent effect (*49*)
Degree heterogeneity	Variation in the number of unweighted connections (edges) across all nodes in a network	+ (*8*)
Node property	**Definition—node level**	**Effect on node susceptibility**
Degree	Number of edges connected to a given node	+ (*49*)
Betweenness centrality (random walk)	Extent to which a node acts as an intermediary for the flow traffic between all other pairs of nodes, when agents travel by random walk	+ (*50*)
Efficiency centrality	Spreading ability of a node, measured as the relative drop in network efficiency caused by its removal	+ (*51*)
Interchamber density	Proportion of other chambers directly connected to a focal chamber	+

overall nest network were affected by treatment (table S1; LMM for clustering and degree heterogeneity: effect of treatment × time, $\chi^2 \leq 0.07$, df = 1, $P \geq 0.51$; effect of treatment at 6 days, $\chi^2 \leq 1.35$, df = 1, $P \geq 0.25$, in all tests). Overall, these results indicate that pathogen exposure leads to multiple changes in the overall topology of the nest networks that should decrease pathogen transmission.

Pathogen exposure influences the topological position of nest chambers

Previous studies of transport and social networks have shown that highly populated nodes and nodes with high network centrality (e.g., degree, betweenness, and efficiency centrality; Table 1) are both at high risk of contamination and are highly influential for the onward spread to the rest of the network (*2*, *33*–*35*). Because nest chambers contain a large portion of the nest population, including valuable and vulnerable colony members such as the queen, young adults, and the brood, we predicted that pathogen-exposed groups would build chambers in positions associated with lower exposure risk and lower spreading ability, characterized by lower network centrality and reduced connections to other chambers.

Most chambers had a degree of three, and neither chamber degree nor betweenness differed between treatments [table S1; Poisson GLMM (degree) and LMM (betweenness), interaction time × treatment and main treatment effects, $\chi^2 \leq 0.03$, df = 1, $P \geq 0.59$, in all tests; Poisson GLMM (degree) and LMM (betweenness) at 6 days, $\chi^2 \leq 0.20$, df = 1, $P \geq 0.66$]. However, in agreement with our prediction, the efficiency centrality of nest chambers tended to decrease faster in pathogen-exposed compared with control nests and was significantly reduced in pathogen-exposed nests by the end of the experiment (Fig. 2; LMM, interaction treatment × time, $\chi^2 = 1.97$, df = 1, $P = 0.16$; Fig. 3A; LMM, effect of treatment at 6 days, $\chi^2 = 6.07$, df = 1, $P = 0.014$). Furthermore, the density of connection of chambers to other chambers decreased significantly faster in pathogen-exposed versus control nests and was significantly reduced in pathogen-exposed nests by 6 days after exposure (Fig. 2; LMM, interaction treatment × time, $\chi^2 = 25.30$, df = 1, $P < 0.0001$; Fig. 3A; LMM, effect of treatment at 6 days, $\chi^2 = 16.02$, df = 1, $P < 0.001$). Altogether, these results indicate that pathogen-exposed ants excavate chambers in positions that should reduce the severity of epidemics.

Pathogen-induced changes in nest architecture decrease disease transmission

Our results so far suggest that pathogen exposure triggers a range of transmission-inhibitory changes in nest architecture by 6 days after initial pathogen exposure (Fig. 3), from the self-isolation of exposed workers to the surface to changes in the geometry and topology of the excavated nests. This could play an important role in preventing epidemics upon later, secondary disease challenges, arising for example from contact with the sporulating bodies of the initially exposed individuals or from new infectious sources in pathogen-rich environments. To formally test the impact of these changes on secondary epidemic risk, we developed an agent-based model that simulated the transmission of an infectious pathogen within the observed nest networks at day 6. This model was inspired from previous models of disease transmission in ant nests (*1*, *2*, *32*) and ant traffic in confined space (*36*, *37*) (materials and methods). In the model, agents moved through the nest and aggregated locally inside nest chambers (*20*, *38*). Pathogen-treated agents initially entered the nest through a randomly selected entrance, and pathogen transmission occurred as a stochastic process between pairs of agents sharing the same within-nest location (chambers, tunnels, dead ends, and junctions). We simulated the transmission of *M. brunneum* over the experimental nest networks extracted 6 days after treatment after a similar disease challenge (20 out of 200 agents), as in our experiments. Relative to simulations of transmission through control nests, simulations of transmission through pathogen-exposed nests resulted in a significant reduction in the amount of spores received by untreated agents and in the proportion of these agents that received a high (more lethal) load (Fig. 4A; LMM interaction treatment × time: median load, $\chi^2 = 102.546$, df = 1, $P < 0.0001$; prevalence of high load, $\chi^2 = 127.24$, df = 1, $P < 0.0001$). Furthermore, we found that the architecture of pathogen-exposed nests inhibited transmission even when only a single pathogen-treated agent was introduced (fig. S4A and table S3), demonstrating the robustness of this effect.

To tease apart the relative importance of different pathogen-induced architectural modifications in reducing transmission, we applied partial least-squares regression to the outcome of simulations over all nests. All properties were found to have the expected effects on transmission: Presumed transmission-inhibitory properties (weighted diameter, unweighted diameter, modularity, and interchamber density)

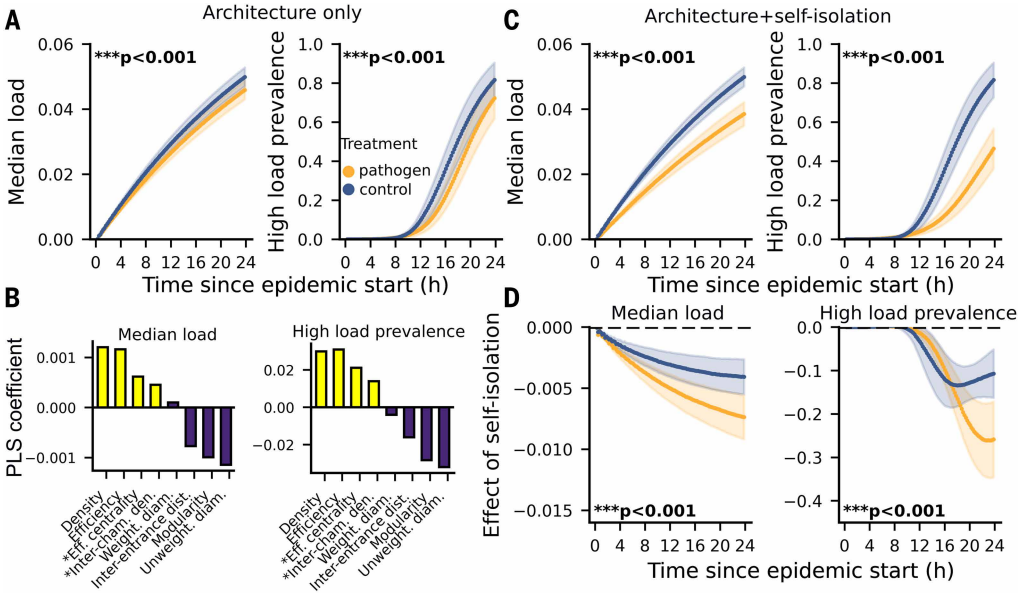

Fig. 4. Agent-based simulations of *M. brunneum* transmission within 6-day nest networks. (**A** and **B**) Simulation outcomes without self-isolation in either treatment group. (**C**) Simulation outcomes with self-isolation of treated agents in pathogen-exposed nests only. (**D**) Difference in simulated transmission with self-isolation versus without self-isolation in both treatment groups. One hundred simulations were performed on each nest for each condition (with or without self-isolation), and cross-simulation means were calculated for each nest every 800 s ($n = 107$ time points), resulting in one data point per nest per time point and per condition. [(A) and (C)] Points and shaded areas represent the grand means and standard errors of the median load (left) and high load prevalence (right) across untreated agents in simulations over control (blue, $n = 10$ per time point) and pathogen-exposed (orange, $n = 10$ per time point) nest networks. (B) Bars indicate coefficients from partial least-squares regression (PLS) analyzing the relative effects of nest network properties targeted by architectural modifications on simulated median load (left) and high load prevalence (right) in the absence of any self-isolation. Positive (resp. negative) values indicate a positive (resp. negative) association between a property and transmission, and bar height is proportional to its relative influence on transmission. Transmission-enhancing properties are indicated in yellow, and transmission-inhibitory properties are indicated in purple. Chamber properties are highlighted by an asterisk; all other properties apply to the global topology of the nest. All pathogen-induced changes were transmission inhibitory. (D) Points and shaded areas represent the grand means and standard errors of the cross-condition differences in median load and high load prevalence (transmission with self-isolation minus transmission without self-isolation; $n = 10$ nests per treatment and per time point). Negative values reflect a transmission-inhibitory effect of self-isolation by treated agents. Details of statistical analyses are provided in table S3.

were negatively associated with transmission, whereas presumed transmission-enhancing properties (density, efficiency, and efficiency centrality) were positively associated with transmission (Fig. 4B). Efficiency, density, unweighted diameter, and modularity (whole-network properties) had the strongest associations with transmission; chamber properties had weaker associations, with efficiency centrality showing a stronger effect on transmission compared with interchamber density; and weighted nest diameter and interentrance distances had the weakest association with transmission (Fig. 4B).

Previous research (*2*) and our surface-activity results (fig. S1) indicate that infectious ants isolate themselves from unexposed nestmates, which reduces transmission risk. To investigate potential interactions between this behavioral response and architectural responses to disease, we repeated our simulations with an additional self-isolation mechanism, whereby pathogen-treated agents displayed an upward movement bias (i.e., increased probability of selecting tunnels connected to higher elevation nodes, such as nest entrances) that led them to spend more time outside the nest (figs. S5 to S7 and table S3). We found that the combined effects of pathogen-induced architectural changes and self-isolation in pathogen-exposed nests resulted in much stronger inhibition of disease transmission compared with architecture alone (Fig. 4C; LMM interaction treatment × time: median load, $\chi^2 = 279.00$, df = 1, $P < 0.0001$; prevalence of high load, $\chi^2 = 212.241$, df = 1, $P < 0.0001$). This was not due to purely additive effects between the two types of responses. Instead, self-isolation was significantly more effective at inhibiting transmission in pathogen-exposed versus control nest architectures (Fig. 4D; LMM interaction treatment × self-isolation × time: median load, $\chi^2 = 37.77$, df = 1, $P < 0.0001$; prevalence of high load, $\chi^2 = 15.19$, df = 1, $P < 0.001$), demonstrating a positive synergy between architectural and behavioral responses, which was robust across a broad range of simulation parameters (fig. S8). Further analyses indicated that this synergy may be a consequence of pathogen-exposed nest networks facilitating the self-isolation of infectious individuals because the same individual-level movement rules (local upward movement bias) tended to result in greater spatial (proportion of time spent outside) and social (network distance between healthy and treated agents) distancing in pathogen-exposed nests (fig. S5 and table S3). Altogether, these results suggest that although the direct effects of pathogen-induced architectural changes on disease transmission are relatively small (Fig. 4A), their indirect effects through synergy with self-isolation are much greater (Fig. 4, C and D), providing enhanced protection against pathogen threats.

Discussion

Group-living animals have evolved collective responses to infectious pathogens that decrease the risk of epidemics (*2*, *9*–*12*). Most responses reported so far involve changes in social interactions between individuals, ranging from social care to self-isolation, social distancing, and social network reorganization (*38*). Our results suggest that these social changes are complemented by spatial modifications to the environment that confer protection against future disease challenges, which had previously only been shown in humans.

Most pathogen-induced changes in architecture increased over time, which could be linked with the nest's development. At the beginning of the experiment, nests were small, which may have limited the scope for implementing architectural changes. At this early stage, self-isolation by pathogen-exposed individuals may therefore be the most effective strategy to prevent the spread of infectious material into the nest. As nests grow larger, with more chambers, junctions, and tunnels, they may become more amenable to topological manipulation, making architectural modification a more potent—and durable—epidemic defense strategy. In fact, the number of possible network configurations scales nonlinearly with the number of nodes (*39*, *40*). By emphasizing social distancing early on and architectural modifications later in nest development, pathogen-exposed ants may dynamically adapt their social immunity to implement the most effective defense. Furthermore, by adopting a transmission-inhibitory nest architecture only after experiencing a real disease challenge, colonies may ensure that efficient flows of resources and information are maintained

throughout the nest in disease-free environments (*41*, *42*). These hypotheses highlight the need to examine pathogen-induced architectural modifications in more natural settings because the limited space and time available in our experimental setup may have curtailed the ability of pathogen-exposed colonies to fully express far-reaching transmission-inhibitory nest modifications.

The mechanisms driving the pathogen-induced changes in nest architecture remain to be established. Although the architectural modifications reported in this work could at least in part arise as an incidental side effect of infection symptoms in diseased workers, it is unlikely to be the sole mechanism at play for three reasons. First, changes to entrance-entrance distance and weighted diameter were detectable as early as 24 hours after exposure. Because *M. brunneum* takes more than 24 hours to enter the host's body and start replicating (*43*), these early changes occurred before the beginning of infection in pathogen-exposed workers and therefore likely reflect an active host response. Second, nests were excavated faster in pathogen-exposed compared with control groups, despite pathogen-exposed workers typically spending less time inside the nest and tending to display reduced activity after exposure, which should decrease excavation rates. This suggests that other mechanisms may be involved. Third, pathogen-treated workers spend much more time near the surface and should thus have less influence on belowground nest morphology compared with other workers. Thus, the topological changes may well involve active shifts in decision-making among untreated workers about where to excavate entrances, chambers, and tunnels. Identifying the fine-grained, individual-level mechanisms that lead to this shift in collective decision-making represents an exciting area of future research.

Overall, our results suggest that ants adjust their nest architecture to reduce colony-wide disease transmission, providing a form of "architectural immunity" that could act as a key component of ant social immunity in pathogen-rich environments (*18*). In addition to uncovering a previously unknown cooperative strategy for avoiding epidemics, our findings provide an example of how social animals may leverage the structure of their built environment to improve their resilience against extrinsic stress, such as extreme temperatures (*24*). Our findings could also have implications beyond animal societies—the architectural changes highlighted in this work have been tuned for effectiveness over long evolutionary time and could serve as a proof of concept or source of inspiration for real-world disease control interventions (*2*, *13*, *44*).

REFERENCES AND NOTES

1. L. Danon, T. A. House, J. M. Read, M. J. Keeling, *J. R. Soc. Interface* **9**, 2826–2833 (2012).
2. N. Stroeymeyt *et al.*, *Science* **362**, 941–945 (2018).
3. I. de Freslon, B. Martínez-López, J. Belkhiria, A. Strappini, G. Monti, *Appl. Anim. Behav. Sci.* **213**, 47–54 (2019).
4. J. A. Tracey, S. N. Bevins, S. VandeWoude, K. R. Crooks, *Ecosphere* **5**, 119 (2014).
5. G. C. Silva, E. M. S. Ribeiro, *Sci. Rep.* **13**, 2240 (2023).
6. S. Uddin, A. Khan, H. Lu, F. Zhou, S. Karim, *Int. J. Environ. Res. Public Health* **19**, 2039 (2022).
7. M. J. Keeling, L. Danon, M. C. Vernon, T. A. House, *Proc. Natl. Acad. Sci. U.S.A.* **107**, 8866–8870 (2010).
8. V. Colizza, A. Barrat, M. Barthélemy, A. Vespignani, *Proc. Natl. Acad. Sci. U.S.A.* **103**, 2015–2020 (2006).
9. J. F. Stephenson, S. E. Perkins, J. Cable, *J. Anim. Ecol.* **87**, 1525–1533 (2018).
10. P. C. Lopes, P. Block, B. König, *Sci. Rep.* **6**, 31790 (2016).
11. N. Bos, T. Lefèvre, A. B. Jensen, P. d'Ettorre, *J. Evol. Biol.* **25**, 342–351 (2012).
12. G. Heiler *et al.*, in *2020 IEEE International Conference on Big Data (Big Data)* (IEEE, 2020), pp. 3123–3132.
13. N. Pinter-Wollman, A. Jelić, N. M. Wells, *Phil. Trans. R. Soc. B* **373**, 20170245 (2018).
14. T. Fisher, *Places J.* 10.22269/101018 (2010).
15. M. Gharipour, A. Tchikine, Eds., *Salutogenic Urbanism: Architecture and Public Health in Early Modern European Cities* (Palgrave Macmillan, 2023).
16. P. Crucitti, V. Latora, S. Porta, *Phys. Rev. E* **73**, 036125 (2006).
17. N. A. Megahed, E. M. Ghoneim, *Sustain Cities Soc.* **61**, 102350 (2020).
18. S. Cremer, S. A. O. Armitage, P. Schmid-Hempel, *Curr. Biol.* **17**, R693–R702 (2007).
19. A. Perna, G. Theraulaz, *J. Exp. Biol.* **220**, 83–91 (2017).
20. N. Stroeymeyt, B. Casillas-Pérez, S. Cremer, *Curr. Opin. Insect Sci.* **5**, 1–15 (2014).
21. S. O'Fallon, E. S. H. Lowell, D. Daniels, N. Pinter-Wollman, *Behav. Ecol.* **33**, 644–653 (2022).
22. N. J. Minter, N. R. Franks, K. A. Brown, *J. R. Soc. Interface* **9**, 586–595 (2012).
23. M. Sankovitz, J. Purcell, *Sci. Rep.* **11**, 23053 (2021).
24. F. García Ibarra, P. Jouquet, N. Bottinelli, A. Bultelle, T. Monnin, *J. Anim. Ecol.* **93**, 319–332 (2024).
25. E. Toffin, J. Kindekens, J.-L. Deneubourg, *Proc. R. Soc. B* **277**, 2617–2625 (2010).
26. J.-B. Leclerc, J. Pinto Silva, C. Detrain, *R. Soc. Open Sci.* **5**, 180267 (2018).
27. C. D. Pull *et al.*, *eLife* **7**, e32073 (2018).
28. A. Reber, M. Chapuisat, *Insectes Soc.* **59**, 231–239 (2012).
29. M. Kim *et al.*, *Bull. World Health Organ.* **98**, 842–848 (2020).
30. P. Rasse, J.-L. Deneubourg, *J. Insect Behav.* **14**, 433–449 (2001).
31. M. Salathé, J. H. Jones, *PLOS Comput. Biol.* **6**, e1000736 (2010).
32. M. L. Mouronte-López, *J. Adv. Transp.* **2021**, 5513311 (2021).
33. E. Dudkina *et al.*, *Int. J. Control* **97**, 1325–1340 (2023).
34. S. M. Kissler *et al.*, *Epidemics* **26**, 86–94 (2019).
35. N. Gravish, G. Gold, A. Zangwill, M. A. Goodisman, D. I. Goldman, *Soft Matter* **11**, 6552–6561 (2015).
36. J. Chang, S. Powell, E. J. H. Robinson, M. C. Donaldson-Matasci, *Swarm Intell.* **15**, 7–30 (2021).
37. T. O. Richardson, N. Stroeymeyt, A. Crespi, L. Keller, *Nat. Commun.* **13**, 6985 (2022).
38. S. Stockmaier *et al.*, *Science* **371**, eabc8881 (2021).
39. A.-L. Barabási, R. Albert, *Science* **286**, 509–512 (1999).
40. N. J. A. Sloane, S. Plouffe, *The Encyclopedia of Integer Sequences* (Academic Press, 1995).
41. M. R. Pie, R. B. Rosengaus, J. F. Traniello, *J. Theor. Biol.* **226**, 45–51 (2004).
42. Z. Cook, D. W. Franks, E. J. H. Robinson, *Behav. Ecol. Sociobiol.* **68**, 509–517 (2014).
43. E. V. Grizanova, C. J. Coates, I. M. Dubovskiy, T. M. Butt, *Virulence* **10**, 999–1012 (2019).
44. J. J. Baljon, J. T. Wilson, *Curr. Opin. Immunol.* **77**, 102215 (2022).
45. V. Latora, M. Marchiori, *Phys. Rev. Lett.* **87**, 198701 (2001).
46. M. Barthélemy, A. Barrat, R. Pastor-Satorras, A. Vespignani, *J. Theor. Biol.* **235**, 275–288 (2005).
47. I. Z. Kiss, D. M. Green, R. R. Kao, *J. R. Soc. Interface* **3**, 669–677 (2006).
48. P. Sah, S. T. Leu, P. C. Cross, P. J. Hudson, S. Bansal, *Proc. Natl. Acad. Sci. U.S.A.* **114**, 4165–4170 (2017).
49. E. M. Volz, J. C. Miller, A. Galvani, L. Ancel Meyers, *PLOS Comput. Biol.* **7**, e1002042 (2011).
50. M. E. J. Newman, *Soc. Networks* **27**, 39–54 (2005).
51. S. Wang, Y. Du, Y. Deng, *Commun. Nonlinear Sci. Numer. Simul.* **47**, 151–163 (2017).
52. L. Leckie, M. S. Andon, K. Bruce, N. Stroeymeyt, Architectural immunity: Ants alter their nest networks to prevent epidemics, Zenodo (2025). https://doi.org/10.5281/zenodo.15353580

ACKNOWLEDGMENTS

We thank L. Martin-Silverstone and the XTM Facility, Palaeobiology Research Group, University of Bristol, for use and training for micro-CT scanning. We thank N. V. Meyling from the University of Copenhagen for providing the *M. brunneum* strain. We also thank A. Perna for advice on how to extract networks from 3D image data and R. Brown, F. Masson, T. Richardson, D. Schläppi, and A. Wanderlingh for comments on the manuscript. **Funding:** This work was supported by the European Research Council (ERC starting grant DISEASE, no. 802628, to N.S.). **Author contributions:** L.L. and N.S. designed the study. M.S.A. and K.B. designed and performed the video analysis. M.S.A., K.B., and L.L. conducted the experiment. L.L. designed the code for the network extraction, agent-based model, analysis, and figure generation, with input from N.S. L.L. and N.S. wrote the manuscript. **Competing interests:** The authors declare no competing interests. **Data and materials availability:** Data are available at Zenodo (*52*). All code is available through Github (https://github.com/Luke-Leckie/Architectural_Immunity_Nest_Networks).

This research was funded in whole or in part by the European Research Council (grant no. 802628); as required the author will make the Author Accepted Manuscript (AAM) version available under a CC BY public copyright license.

SUPPLEMENTARY MATERIALS

science.org/doi/10.1126/science.ads5930
Materials and Methods; Supplementary Text; Figs. S1 to S11; Tables S1 to S4; References (*53*–*64*); Movie S1

Submitted 20 August 2024; resubmitted 23 January 2025; accepted 12 August 2025
10.1126/science.ads5930